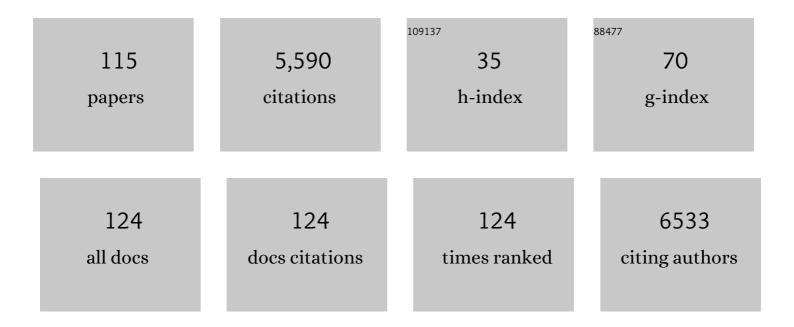
Marc Simard

List of Publications by Year in descending order

Source: https://exaly.com/author-pdf/6913542/publications.pdf Version: 2024-02-01



#	Article	IF	CITATIONS
1	Mapping forest canopy height globally with spaceborne lidar. Journal of Geophysical Research, 2011, 116, .	3.3	855
2	Distribution and drivers of global mangrove forest change, 1996–2010. PLoS ONE, 2017, 12, e0179302.	1.1	380
3	Mangrove canopy height globally related to precipitation, temperature and cyclone frequency. Nature Geoscience, 2019, 12, 40-45.	5.4	279
4	Mapping Height and Biomass of Mangrove Forests in Everglades National Park with SRTM Elevation Data. Photogrammetric Engineering and Remote Sensing, 2006, 72, 299-311.	0.3	240
5	The use of decision tree and multiscale texture for classification of JERS-1 SAR data over tropical forest. IEEE Transactions on Geoscience and Remote Sensing, 2000, 38, 2310-2321.	2.7	158
6	Research Trends in the Use of Remote Sensing for Inland Water Quality Science: Moving Towards Multidisciplinary Applications. Water (Switzerland), 2020, 12, 169.	1.2	156
7	Representing the function and sensitivity of coastal interfaces in Earth system models. Nature Communications, 2020, 11, 2458.	5.8	153
8	Biomass estimation from simulated GEDI, ICESat-2 and NISAR across environmental gradients in Sonoma County, California. Remote Sensing of Environment, 2020, 242, 111779.	4.6	152
9	Height and biomass of mangroves in Africa from ICESat/GLAS and SRTM. International Journal of Remote Sensing, 2013, 34, 668-681.	1.3	146
10	A systematic method for 3D mapping of mangrove forests based on Shuttle Radar Topography Mission elevation data, ICEsat/GLAS waveforms and field data: Application to Ciénaga Grande de Santa Marta, Colombia. Remote Sensing of Environment, 2008, 112, 2131-2144.	4.6	139
11	A Temporal Decorrelation Model for Polarimetric Radar Interferometers. IEEE Transactions on Geoscience and Remote Sensing, 2012, 50, 2880-2888.	2.7	137
12	A comprehensive benchmarking system for evaluating global vegetation models. Biogeosciences, 2013, 10, 3313-3340.	1.3	119
13	Landscapeâ€scale extent, height, biomass, and carbon estimation of Mozambique's mangrove forests with Landsat ETM+ and Shuttle Radar Topography Mission elevation data. Journal of Geophysical Research, 2008, 113, .	3.3	114
14	Aboveground biomass density models for NASA's Global Ecosystem Dynamics Investigation (GEDI) lidar mission. Remote Sensing of Environment, 2022, 270, 112845.	4.6	108
15	Fusing simulated GEDI, ICESat-2 and NISAR data for regional aboveground biomass mapping. Remote Sensing of Environment, 2021, 253, 112234.	4.6	99
16	Analysis of speckle noise contribution on wavelet decomposition of SAR images. IEEE Transactions on Geoscience and Remote Sensing, 1998, 36, 1953-1962.	2.7	90
17	A remote sensing-based model of tidal marsh aboveground carbon stocks for the conterminous United States. ISPRS Journal of Photogrammetry and Remote Sensing, 2018, 139, 255-271.	4.9	89
18	A general framework for propagule dispersal in mangroves. Biological Reviews, 2019, 94, 1547-1575.	4.7	88

#	Article	IF	CITATIONS
19	AquaSat: A Data Set to Enable Remote Sensing of Water Quality for Inland Waters. Water Resources Research, 2019, 55, 10012-10025.	1.7	78
20	Global-scale dispersal and connectivity in mangroves. Proceedings of the National Academy of Sciences of the United States of America, 2019, 116, 915-922.	3.3	75
21	Mapping tropical coastal vegetation using JERS-1 and ERS-1 radar data with a decision tree classifier. International Journal of Remote Sensing, 2002, 23, 1461-1474.	1.3	73
22	Scaling mangrove aboveground biomass from siteâ€level to continentalâ€scale. Global Ecology and Biogeography, 2016, 25, 286-298.	2.7	73
23	The role of economic, policy, and ecological factors in estimating the value of carbon stocks in Everglades mangrove forests, South Florida, USA. Environmental Science and Policy, 2016, 66, 160-169.	2.4	72
24	The Role of the Everglades Mangrove Ecotone Region (EMER) in Regulating Nutrient Cycling and Wetland Productivity in South Florida. Critical Reviews in Environmental Science and Technology, 2011, 41, 633-669.	6.6	64
25	Harnessing Big Data to Support the Conservation and Rehabilitation of Mangrove Forests Globally. One Earth, 2020, 2, 429-443.	3.6	63
26	Achieving accuracy requirements for forest biomass mapping: A spaceborne data fusion method for estimating forest biomass and LiDAR sampling error. Remote Sensing of Environment, 2013, 130, 153-170.	4.6	58
27	The Global Rain Forest Mapping Project JERS-1 radar mosaic of tropical Africa: development and product characterization aspects. IEEE Transactions on Geoscience and Remote Sensing, 2000, 38, 2218-2233.	2.7	56
28	Airborne Laser Scanning Quantification of Disturbances from Hurricanes and Lightning Strikes to Mangrove Forests in Everglades National Park, USA. Sensors, 2008, 8, 2262-2292.	2.1	53
29	Mapping Migratory Bird Prevalence Using Remote Sensing Data Fusion. PLoS ONE, 2012, 7, e28922.	1.1	53
30	Contribution of L-band SAR to systematic global mangrove monitoring. Marine and Freshwater Research, 2014, 65, 589.	0.7	52
31	A Comparison of Mangrove Canopy Height Using Multiple Independent Measurements from Land, Air, and Space. Remote Sensing, 2016, 8, 327.	1.8	52
32	The UAVSAR instrument: Description and first results. , 2008, , .		48
33	An Empirical Assessment of Temporal Decorrelation Using the Uninhabited Aerial Vehicle Synthetic Aperture Radar over Forested Landscapes. Remote Sensing, 2012, 4, 975-986.	1.8	47
34	Partitioning the relative contributions of organic matter and mineral sediment to accretion rates in carbonate platform mangrove soils. Marine Geology, 2017, 390, 170-180.	0.9	46
35	NASADEM GLOBAL ELEVATION MODEL: METHODS AND PROGRESS. International Archives of the Photogrammetry, Remote Sensing and Spatial Information Sciences - ISPRS Archives, 0, XLI-B4, 125-128.	0.2	45
36	NASADEM GLOBAL ELEVATION MODEL: METHODS AND PROGRESS. International Archives of the Photogrammetry, Remote Sensing and Spatial Information Sciences - ISPRS Archives, 0, XLI-B4, 125-128.	0.2	42

#	Article	IF	CITATIONS
37	Large-scale vegetation maps derived from the combined L-band GRFM and C-band CAMP wide area radar mosaics of Central Africa. International Journal of Remote Sensing, 2002, 23, 1261-1282.	1.3	39
38	An Assessment of Temporal Decorrelation Compensation Methods for Forest Canopy Height Estimation Using Airborne L-Band Same-Day Repeat-Pass Polarimetric SAR Interferometry. IEEE Journal of Selected Topics in Applied Earth Observations and Remote Sensing, 2018, 11, 95-111.	2.3	39
39	Canopy Height Model (CHM) Derived From a TanDEM-X InSAR DSM and an Airborne Lidar DTM in Boreal Forest. IEEE Journal of Selected Topics in Applied Earth Observations and Remote Sensing, 2016, 9, 381-397.	2.3	38
40	Radarsat-2 Backscattering for the Modeling of Biophysical Parameters of Regenerating Mangrove Forests. Remote Sensing, 2015, 7, 17097-17112.	1.8	36
41	Improving mangrove above-ground biomass estimates using LiDAR. Estuarine, Coastal and Shelf Science, 2020, 236, 106585.	0.9	33
42	The NASA AfriSAR campaign: Airborne SAR and lidar measurements of tropical forest structure and biomass in support of current and future space missions. Remote Sensing of Environment, 2021, 264, 112533.	4.6	33
43	Large-Scale High-Resolution Coastal Mangrove Forests Mapping Across West Africa With Machine Learning Ensemble and Satellite Big Data. Frontiers in Earth Science, 2021, 8, .	0.8	31
44	New perspectives on global ecosystems from wide-area radar mosaics: Flooded forest mapping in the tropics. International Journal of Remote Sensing, 2000, 21, 1235-1249.	1.3	29
45	Improving the Transferability of Suspended Solid Estimation in Wetland and Deltaic Waters with an Empirical Hyperspectral Approach. Remote Sensing, 2019, 11, 1629.	1.8	29
46	A review of carbon monitoring in wet carbon systems using remote sensing. Environmental Research Letters, 2022, 17, 025009.	2.2	29
47	Radiometric Correction of Airborne Radar Images Over Forested Terrain With Topography. IEEE Transactions on Geoscience and Remote Sensing, 2016, 54, 4488-4500.	2.7	26
48	Forest Height Estimation Using Multibaseline PolInSAR and Sparse Lidar Data Fusion. IEEE Journal of Selected Topics in Applied Earth Observations and Remote Sensing, 2018, 11, 3415-3433.	2.3	26
49	Highâ€resolution forest canopy height estimation in an African blue carbon ecosystem. Remote Sensing in Ecology and Conservation, 2015, 1, 51-60.	2.2	24
50	An Error Model for Biomass Estimates Derived From Polarimetric Radar Backscatter. IEEE Transactions on Geoscience and Remote Sensing, 2014, 52, 4065-4082.	2.7	23
51	Mapping boreal forest biomass from a SRTM and TanDEM-X based on canopy height model and Landsat spectral indices. International Journal of Applied Earth Observation and Geoinformation, 2018, 68, 202-213.	1.4	23
52	High-resolution mapping of biomass and distribution of marsh and forested wetlands in southeastern coastal Louisiana. International Journal of Applied Earth Observation and Geoinformation, 2019, 80, 257-267.	1.4	23
53	Retrieval of Forest Vertical Structure from PolInSAR Data by Machine Learning Using LIDAR-Derived Features. Remote Sensing, 2019, 11, 381.	1.8	21
54	Integrating Imaging Spectrometer and Synthetic Aperture Radar Data for Estimating Wetland Vegetation Aboveground Biomass in Coastal Louisiana. Remote Sensing, 2019, 11, 2533.	1.8	20

#	Article	IF	CITATIONS
55	Sex-specific perinatal expression of glutathione peroxidases during mouse lung development. Molecular and Cellular Endocrinology, 2012, 355, 87-95.	1.6	19
56	An approach to monitoring mangrove extents through time-series comparison of JERS-1 SAR and ALOS PALSAR data. Wetlands Ecology and Management, 2015, 23, 3-17.	0.7	19
57	Imaging Spectroscopy BRDF Correction for Mapping Louisiana's Coastal Ecosystems. IEEE Transactions on Geoscience and Remote Sensing, 2018, 56, 1739-1748.	2.7	19
58	Mangrove carbon stocks in Pongara National Park, Gabon. Estuarine, Coastal and Shelf Science, 2021, 259, 107432.	0.9	19
59	Deformation, Ecosystem Structure, and Dynamics of Ice (DESDynI). Aerospace Conference Proceedings IEEE, 2008, , .	0.0	18
60	Using InSAR Coherence to Map Stand Age in a Boreal Forest. Remote Sensing, 2013, 5, 42-56.	1.8	18
61	Allometric Scaling and Resource Limitations Model of Tree Heights: Part 1. Model Optimization and Testing over Continental USA. Remote Sensing, 2013, 5, 284-306.	1.8	18
62	Allometric Scaling and Resource Limitations Model of Tree Heights: Part 3. Model Optimization and Testing over Continental China. Remote Sensing, 2014, 6, 3533-3553.	1.8	17
63	Adaptation of the Wavelet Transform for the Construction of Multiscale Texture Maps of SAR Images. Canadian Journal of Remote Sensing, 1998, 24, 264-285.	1.1	15
64	Allometric Scaling and Resource Limitations Model of Tree Heights: Part 2. Site Based Testing of the Model. Remote Sensing, 2013, 5, 202-223.	1.8	15
65	Analysis of Floodplain Dynamics in the Atrato River Colombia Using SAR Interferometry. Water (Switzerland), 2019, 11, 875.	1.2	15
66	Mapping Water Surface Elevation and Slope in the Mississippi River Delta Using the AirSWOT Ka-Band Interferometric Synthetic Aperture Radar. Remote Sensing, 2019, 11, 2739.	1.8	15
67	Monitoring Water Level Change and Seasonal Vegetation Change in the Coastal Wetlands of Louisiana Using L-Band Time-Series. Remote Sensing, 2020, 12, 2351.	1.8	15
68	Residual motion estimation for UAVSAR: Implications of an electronically scanned array. , 2009, , .		14
69	Mapping forest canopy height using TanDEM-X DSM and airborne LiDAR DTM. , 2014, , .		14
70	A Lidar-Radar Framework to Assess the Impact of Vertical Forest Structure on Interferometric Coherence. IEEE Journal of Selected Topics in Applied Earth Observations and Remote Sensing, 2016, 9, 5830-5841.	2.3	13
71	The 2016 NASA AfriSAR campaign: Airborne SAR and Lidar measurements of tropical forest structure and biomass in support of future satellite missions. , 2017, , .		13
72	Aboveground biomass distributions and vegetation composition changes in Louisiana's Wax Lake Delta. Estuarine, Coastal and Shelf Science, 2021, 250, 107139.	0.9	13

#	Article	lF	CITATIONS
73	Continental-Scale Canopy Height Modeling by Integrating National, Spaceborne, and Airborne LiDAR Data. Canadian Journal of Remote Sensing, 2016, 42, 574-590.	1.1	12
74	Monitoring Forest Loss in ALOS/PALSAR Time-Series with Superpixels. Remote Sensing, 2019, 11, 556.	1.8	11
75	Initial results from the 2019 NISAR Ecosystem Cal/Val Exercise in the SE USA. , 2019, , .		10
76	Structural Characteristics of the Tallest Mangrove Forests of the American Continent: A Comparison of Ground-Based, Drone and Radar Measurements. Frontiers in Forests and Global Change, 2021, 4, .	1.0	10
77	Leveraging the Historical Landsat Catalog for a Remote Sensing Model of Wetland Accretion in Coastal Louisiana. Journal of Geophysical Research G: Biogeosciences, 2022, 127, .	1.3	9
78	Integrating Connectivity Into Hydrodynamic Models: An Automated Openâ€Source Method to Refine an Unstructured Mesh Using Remote Sensing. Journal of Advances in Modeling Earth Systems, 2022, 14, .	1.3	9
79	Polinsar forestry applications improved by modeling height-dependent temporal decorrelation. , 2010, , .		8
80	Application of the metabolic scaling theory and water–energy balance equation to model largeâ€scale patterns of maximum forest canopy height. Global Ecology and Biogeography, 2016, 25, 1428-1442.	2.7	8
81	Kapok: An open source python library for polinsar forest height estimation using uavsar data. , 2017, , .		8
82	InSAR Phase Unwrapping Error Correction for Rapid Repeat Measurements of Water Level Change in Wetlands. IEEE Transactions on Geoscience and Remote Sensing, 2022, 60, 1-15.	2.7	8
83	Validation of the new SRTM digital elevation model (NASADEM) with ICESAT/GLAS over the United States. , 2016, , .		7
84	The effects of temporal decorrelation and topographic slope on forest height retrieval using airborne repeat-pass L-band polarimetric SAR interferometry. , 2016, , .		7
85	Regional Tropical Aboveground Biomass Mapping with L-Band Repeat-Pass Interferometric Radar, Sparse Lidar, and Multiscale Superpixels. Remote Sensing, 2020, 12, 2048.	1.8	7
86	Comprehensive comparison of airborne and spaceborne SAR and LiDAR estimates of forest structure in the tallest mangrove forest on earth. Science of Remote Sensing, 2021, 4, 100034.	2.2	7
87	L-band and P-band studies of vegetation at JPL. , 2015, , .		6
88	Effects of TanDEM-X Acquisition Parameters on the Accuracy of Digital Surface Models of a Boreal Forest Canopy. Canadian Journal of Remote Sensing, 2017, 43, 194-207.	1.1	6
89	Using rapid repeat SAR interferometry to improve hydrodynamic models of flood propagation in coastal wetlands. Advances in Water Resources, 2022, 159, 104088.	1.7	6
90	Classification of the Gabon SAR mosaic using a wavelet based rule classifier. , 0, , .		5

#	Article	IF	CITATIONS
91	Large-scale mangrove canopy height map generation from TanDEM-X data by means of Pol-InSAR techniques. , 2015, , .		5
92	Orinoco: Retrieving a River Delta Network with the Fast Marching Method and Python. ISPRS International Journal of Geo-Information, 2020, 9, 658.	1.4	5
93	An Improved Scheme for Correcting Remote Spectral Surface Reflectance Simultaneously for Terrestrial BRDF and Waterâ€Surface Sunglint in Coastal Environments. Journal of Geophysical Research G: Biogeosciences, 2022, 127, .	1.3	5
94	Airborne Laser Mapping of Mangroves on the Biscayne Bay Coast, Miami, Florida. , 2006, , .		4
95	Use of Airborne LIDAR for the Assessment of Landscape Structure in the Pine Forests of Everglades National Park. , 2006, , .		4
96	Integrated instrument simulator suites for Earth science. Proceedings of SPIE, 2012, , .	0.8	4
97	Numerical investigation of the effects of distributary bathymetry and roughness on tidal hydrodynamics of Wax Lake region under calm conditions. Estuarine, Coastal and Shelf Science, 2022, 265, 107694.	0.9	4
98	Spatial Patterns of Deltaic Deposition/Erosion Revealed by Streaklines Extracted From Remotelyâ€Sensed Suspended Sediment Concentration. Geophysical Research Letters, 2022, 49, .	1.5	4
99	Atmospheric Lengthscales for Global VSWIR Imaging Spectroscopy. Journal of Geophysical Research G: Biogeosciences, 2022, 127, .	1.3	4
100	Uavsar L-Band and P-Band Tomographic Experiments in Boreal Forests. , 2018, , .		3
101	Hadron production in central heavy-ion collisions. Physical Review D, 1984, 30, 225-227.	1.6	2
102	Snow Water Equivalent retrieval using P-band signals of Opportunity. , 2016, , .		2
103	Prediction of forest canopy structure from PolInSAR dataset. , 2017, , .		2
104	Object-Oriented Monitoring of Forest Disturbances with ALOS/PALSAR Time-Series. , 2019, , .		2
105	Improving Channel Hydrological Connectivity in Coastal Hydrodynamic Models With Remotely Sensed Channel Networks. Journal of Geophysical Research F: Earth Surface, 2022, 127, .	1.0	2
106	Comparison of a decision tree and maximum likelihood classifiers: application to SAR image of tropical forest. , 0, , .		1
107	Using Shuttle Radar Topography Mission Elevation Data to Map Mangrove Forest Height in the Caribbean. , 2006, , .		1
108	Evaluating Current and Future Sensor-Specific Biomass Calibration in the Tallest Mangrove Forest on Earth. , 2020, , .		1

#	Article	IF	CITATIONS
109	A Regional L-Band High Biomass Estimation Framework Leveraging Spaceborne Lidar and Interferometric Data to Overcome Backscatter Saturation. , 2020, , .		1
110	Real-time radar interferometry of ocean surface height. , 2004, 5238, 192.		0
111	Real-Time Processing Algorithm for Wide Swath Radar Interferometry of Ocean Surface. , 2006, , .		0
112	Watershed scale analyses of land cover change in the contributing upland area of mangrove ecosystems. , 2014, , .		0
113	Remote Sensing of Wetland Types: Mangroves. , 2018, , 1641-1647.		0
114	Remote Sensing of Wetland Types: Mangroves. , 2016, , 1-6.		0
115	Mangrove Mapping with the Freeman-Durden Polarimetric Decomposition and Insar Coherence from ALOS-2. , 2020, , .		0